Equilibrium self-assembly of colloids with distinct interaction sites: Thermodynamics, percolation, and cluster distribution functions

J. M. Tavares,[1,2] P. I. C. Teixeira,[1,2,a)] M. M. Telo da Gama,[2,3] and F. Sciortino[4]
[1]*Instituto Superior de Engenharia de Lisboa, Rua Conselheiro Emídio Navarro 1, P-1950-062 Lisbon, Portugal*
[2]*Centro de Física Teórica e Computacional, Avenida Professor Gama Pinto 2, P-1649-003 Lisbon, Portugal*
[3]*Departamento de Física, Faculdade de Ciências da Universidade de Lisboa, P-1749-016 Lisbon, Portugal*
[4]*Dipartimento di Fisica and CNR-ISC, Università di Roma La Sapienza, Piazzale Moro 5, I-00185 Rome, Italy*

(Received 17 February 2010; accepted 4 May 2010; published online 15 June 2010)

We calculate the equilibrium thermodynamic properties, percolation threshold, and cluster distribution functions for a model of associating colloids, which consists of hard spherical particles having on their surfaces three short-ranged attractive sites (sticky spots) of two different types, *A* and *B*. The thermodynamic properties are calculated using Wertheim's perturbation theory of associating fluids. This also allows us to find the onset of self-assembly, which can be quantified by the maxima of the specific heat at constant volume. The percolation threshold is derived, under the no-loop assumption, for the correlated bond model: In all cases it is two percolated phases that become identical at a critical point, when one exists. Finally, the cluster size distributions are calculated by mapping the model onto an effective model, characterized by a—state-dependent—functionality $\bar{f}$ and unique bonding probability $\bar{p}$. The mapping is based on the asymptotic limit of the cluster distributions functions of the generic model and the effective parameters are defined through the requirement that the equilibrium cluster distributions of the true and effective models have the same number-averaged and weight-averaged sizes at all densities and temperatures. We also study the model numerically in the case where *BB* interactions are missing. In this limit, *AB* bonds either provide branching between *A*-chains (Y-junctions) if $\epsilon_{AB}/\epsilon_{AA}$ is small, or drive the formation of a hyperbranched polymer if $\epsilon_{AB}/\epsilon_{AA}$ is large. We find that the theoretical predictions describe quite accurately the numerical data, especially in the region where Y-junctions are present. There is fairly good agreement between theoretical and numerical results both for the thermodynamic (number of bonds and phase coexistence) and the connectivity properties of the model (cluster size distributions and percolation locus). © *2010 American Institute of Physics*. [doi:10.1063/1.3435346]

I. INTRODUCTION

Recent advances in the chemical synthesis and fabrication of nanometer-to-micrometer sized particles have produced a wide variety of new designs. One challenge is to organize them into structures for functional materials and devices. A promising approach is self-assembly, which is the spontaneous organization of matter into ordered arrangements. However, fundamental understanding of the basic principles of self-assembly is lacking and a systematic study of the phase behavior, vitrification, and gelation is needed. The goal is to tailor their behavior at the macroscopic level through the control of the interactions and the self-assembly process.[1–4]

Here we investigate the thermodynamic and structural properties of model patchy colloids, a new generation of colloidal particles the surfaces of which are patterned so that they attract each other via discrete sites of tunable number, size, and strength. More generally, models consisting of hard particles with attractive sites, or patches, on their surfaces, are suitable to investigate the interplay between condensation and clustering, e.g., in protein solutions or strongly dipolar fluids,[5] and have also been extensively used to model pure or mixed chain molecules, e.g., in industrial contexts.[6] They provide a route to designing ideal gels,[7] as well as robust control of a wide range of equilibrium self-assembled structures. Percolation—a prerequisite for gelation—is a geometrical property related to the global connectivity of a system, not described by the thermodynamics, hence we require a statistical theory in order to address this question.

A remarkable theory of interaction site models of association was developed by Wertheim[8–11] some 25 years ago. Although Wertheim's model is based on site-site interactions, he avoided a reduction to a level of description where the sites replace the particles as the primary units.[12] The opposite limit, where the association products are treated as molecules with internal degrees of freedom, while desirable as it provides a structural description, very quickly becomes prohibitively complicated.[13–15] Wertheim's original approach is best described as one in which there are several species of par-

a)Electronic mail: piteixeira@cii.fc.ul.pt.

ticles, each representing a monomeric unit where a specified type of attraction site is bonded. The decision whether a site is bonded is not made by appealing to the idea of physical cluster as in the molecular approaches.[16] Instead it relies on using graph theory after writing the total pair potential as a sum of core-core and site-site potentials and introducing Mayer f-functions for the individual terms.[8–10] This provides a simple expression for the free energy of bond formation, F_b, and lends itself to physically transparent approximations that are exact in the zero-density, strong-association limit. In this limit the theory describes a polydisperse mixture of (possibly branched) polymers;[11] for arbitrary association strengths it yields a versatile description of the thermodynamics of associating systems.

The statistical or molecular approach, on the other hand, was used to study percolation in the context of gelation of polymeric systems. The earliest of these is Flory's random model of polymerization, where monomers with f identical functional groups A, react randomly to form a mixture of polydisperse branched polymers.[13,14] The model may be cast as a random bond percolation model[17–19] and has been solved exactly. A related model, which has also been solved, is the random hyperbranched $A_{f-1}B$ polymer model, where monomers with $f-1$ functional groups of type A and one functional group of type B, react randomly with the restriction that the A groups on one monomer react only with B groups on a different monomer, and vice versa.[18,20] Both of these models are characterized by a single bonding probability, p; generalization of the molecular approach to systems with distinct bonds is quite formidable.

The role of physical clusters of particles in the thermodynamics has been addressed in many different contexts. In particular, Coniglio[21] extended Hill's original work and proposed a general theory of the equilibrium distribution of physical clusters, establishing a relation between percolation (formation of an infinite cluster) and condensation: For systems with attractive interactions, an infinite cluster of particles will appear in the gaseous phase as a prerequisite for condensation.

Patchy colloidal systems open up the possibility of depressing the critical point, thereby providing the means of controlling the bond lifetime of the percolated networks. Indeed in a recent line of work,[22–24] the phase diagram and percolation threshold of patchy colloids with identical interaction sites have been investigated. This is a site-bond correlated model with cluster distribution and percolation threshold that are well described by the Flory–Stockmayer theory[13,14,18] and bonding probabilities that are given almost exactly by Wertheim's thermodynamic perturbation theory for associating fluids.[8–11] Extensive computer simulations established that the number of bonding sites per particle (its *functionality* or *valence*), f, is the key parameter controlling the location of the liquid-vapor critical point: In the limit of average functionality, $\langle f \rangle$, approaching two, the phase-separation region shrinks to zero and it becomes possible to reach low temperatures without encountering phase separation. Recent calculations suggest that cooling the colloidal system can freeze in place the empty configuration to give a glassy state of arbitrarily low density: an ideal (reversible) gel.[22,24]

A generalized version of the model allows for a much deeper understanding of the onset of criticality in low-functionality systems.[25,26] The new model consists of particles decorated with three interacting sites, which are associated with different energy scales, making it possible to go from independent chains to hyperbranched polymers and to simple dimer association. Two sites are of type A and interaction strength ϵ_{AA}, one is of type B and interaction strength ϵ_{BB}. Unlike sites also interact with strength ϵ_{AB}. We found that when two of the three interaction strengths vanish simultaneously, there can be no liquid-vapor critical point. These correspond to the well-known limits of noninteracting linear chains ($\epsilon_{AA} \neq 0$, $\epsilon_{AB}=\epsilon_{BB}=0$), dimers ($\epsilon_{BB} \neq 0$, $\epsilon_{AA}=\epsilon_{AB}=0$), and hyperbranched polymers ($\epsilon_{AB} \neq 0$, $\epsilon_{AA}=\epsilon_{BB}=0$). The detailed fashion in which the critical temperature vanishes as the bonding energies, ϵ_{AB} and ϵ_{BB}, decrease toward zero depends on the order in which the limits $\epsilon_{AB} \to 0$ and $\epsilon_{BB} \to 0$ are taken, which in turn determine the type of network that is formed. Our choice of two A sites and one B site is the simplest that allows exploration of the three above limits, as well as detailed investigation of the interplay between condensation[26] and percolation[27] in these systems. Further generalizations are possible to any number of sites of any number of types, but which are beyond the scope of this paper.

More recently, some of us have calculated the percolation threshold and the lowest-order moments of the cluster size distribution of the general model.[27] The problem was solved exactly under Flory's no-loop assumption and Wertheim's theory was used to provide the connection with equilibrium thermodynamics. Here, we obtain explicit results for a system of colloidal particles with three distinct sites, two of type A and one of type B. The onset of self-assembly, defined by the locus of the maxima of the specific heat at constant volume,[28] is investigated, and a hierarchy of ordering processes is established: At the highest temperature and lowest density, it starts with the self-assembly process of the dominant bonds, followed by self-assembly of the subdominant bonds. The latter process is a prerequisite for the development of a spanning cluster. We find that the percolation transition driven by attractive interactions is a prerequisite for the emergence of criticality and condensation. In all cases it is two percolated phases that become identical at the critical point, when one exists. Farther from the critical point, coexistence is between a dense percolating system and a low-density gas of clusters.

We calculate the cluster size distributions by mapping the model onto an effective model, characterized by a—state-dependent—functionality $\bar{f}$ and a unique bonding probability $\bar{p}$. The mapping is based on the asymptotic limit of the cluster distributions functions of the generic model, and the effective parameters are defined through the requirement that the equilibrium cluster distributions of the true and effective models have the same number- and weight-averaged sizes, at all densities and temperatures. Finally, we report numerical simulations of the model for the case ϵ_{BB}

=0, for several values of the temperature, density, and $\epsilon_{AB}/\epsilon_{AA}$ ratio, to provide an accurate test of the theoretical predictions.

This paper is organized as follows: In Sec. II we describe our model (Sec. II A), Wertheim's thermodynamic perturbation theory as applied to it (Sec. II B), and our treatment of percolation and cluster size distributions (Sec. II C). Details of the simulations are given in Sec. III. Our results for the phase diagrams, critical parameters, percolation lines, and cluster size distributions are presented and discussed in Sec. IV. In Sec. V we conclude and place our results in the context of the wider study of associating fluids, in particular, strongly dipolar fluids. Some useful analytical expressions not found in literature are collected in Appendixes A and B.

II. THEORY

A. The model

Our model is a fluid of N hard spheres (HSs) of diameter σ and volume $v_s=(\pi/6)\sigma^3$, each decorated with three bonding sites (or sticky spots) on its surface. Two of these spots are identical and labeled A, while the third is different and labeled B. In general, two spheres may form bonds of types AA, BB, or AB. Each bond corresponds to a short-ranged attractive interaction between two bonding sites, which is treated as a perturbation of the HS potential. We assume that these potentials are square wells, with depths $\epsilon_{\alpha\beta}$ (where $\alpha,\beta=A,B$), and the interaction range is chosen to be $\delta=0.1196\sigma$, the same for all sites. This is the largest value that still ensures, for geometrical reasons, that each bonding site can only take part in one bond. The theory does not actually require us to specify the positions of the bonding sites over the surface of the sphere, only that they should be arranged in such a way that it is not possible to have more than one bond between any two particles. Of course, in the simulations one needs to specify the site positions. Selecting the A sites on the two poles and the B site on the equator of the particle, the system would form linear chains of AA bonds, branching orthogonally via AB bonds. Since sequences of closed bond loops are not accounted for in Wertheim's first-order perturbation theory[8,9]—and should therefore be avoided when testing its quality—we decided to locate the sites in a geometry that would rule against the formation of, at least, small bond loops, i.e., against triangular and square arrangements of bonded particles. For this reason, we have increased the angle between the A and B sites from 90° (which would favor the formation of perfect squares) to 105°. Hence, if we take the particle center as the origin of an axes frame, the two A sites are located at $([\sigma/2]\sin[\pi/12], \pm[\sigma/2]\cos[\pi/12], 0)$ and the B site at $(-[\sigma/2], 0, 0)$. We stress that a different site geometry would not have made any significant difference to the results[24] affecting mostly the persistence length of the chains.

B. Thermodynamics

For the present model, a fluid of identical spheres with two A and one B bonding sites satisfying the assumptions of Wertheim's theory,[8,9,29] the bonding free energy, F_b, is given by[29]

$$\beta f_b \equiv \frac{\beta F_b}{N} = 2\ln X_A + \ln X_B - X_A - \frac{X_B}{2} + \frac{3}{2}, \tag{1}$$

where $\beta \equiv 1/(k_B T)$, T is the temperature, k_B is the Boltzmann constant, and X_α is the probability of having a sticky spot of type α *not* bonded. $p_\alpha = 1 - X_\alpha$ ($\alpha = A, B$) is thus the fraction of bonding sites of type α that do take part in bonds. The variables X_α are related to the density and temperature through the laws of mass action that are derived by treating bond formation as a chemical reaction. We recall that this is equivalent to disregarding loops in finite branched clusters, thus preserving only pair correlations.[13] The latter are not independent if there is more than a single bonding probability but the bonding sites remain uncorrelated; longer-range correlations, including intracluster self-avoidance, are neglected. The intercluster excluded volume is taken into account through the reference fluid entropic term. It should be noted that more general versions of Wertheim's theory exist that are able to deal with ring formation[30] and bond cooperativity,[31] but these are not consistent with our analysis of cluster sizes and percolation.[32]

The law of mass action then yields the following two equations:[8,9,29]

$$X_A + 2\eta\Delta_{AA}X_A^2 + \eta\Delta_{AB}X_A X_B = 1, \tag{2}$$

$$X_B + \eta\Delta_{BB}X_B^2 + 2\eta\Delta_{AB}X_A X_B = 1, \tag{3}$$

where $\eta \equiv (N/V)v_s$ is the packing fraction and

$$\Delta_{\alpha\beta} = \frac{1}{v_s}\int_{v_{\alpha\beta}} g_{\mathrm{ref}}(\mathbf{r})[\exp(\beta\epsilon_{\alpha\beta}) - 1]d\mathbf{r}. \tag{4}$$

This integral is calculated over $v_{\alpha\beta}$, the volume of bond $\alpha\beta$, and g_{ref} is the pair correlation function (PCF) of the reference system. $f_\alpha f_\beta \Delta_{\alpha\beta}/(1+\delta_{\alpha\beta})$ (with $f_A=2$ and $f_B=1$ the numbers of A and B sites per particle and $\delta_{\alpha\beta}$ the Kronecker delta) plays the role of the equilibrium constant for the reaction between sites α and β.[33] These equations yield the probability $p_\alpha = 1 - X_\alpha$ that a site of type α is bonded, as a function of density, temperature, and the interaction strengths. As we shall see, this enables us to calculate *structural* properties—the percolation threshold—in addition to thermodynamic properties—the self-assembly line, given by the locus of maxima of the specific heat at constant volume.

Here, we shall take all bonds to have the same volume, $v_{\alpha\beta}=v_b$. The reference system is chosen to be the HS fluid, and the following linear approximation[34] is used for the PCF in the range where bonding occurs ($\sigma < r < \sigma+\delta$),

$$g_{\mathrm{ref}}(r) = \frac{1 - \frac{\eta}{2} - \frac{9}{2}\eta(1+\eta)\left(\frac{r-\sigma}{\sigma}\right)}{(1-\eta)^3}. \tag{5}$$

This was used in an earlier work on the model with identical sites, and shown to yield good agreement with simulation.[22,24] Within these two approximations, Eq. (4) becomes

$$\Delta_{\alpha\beta} = \frac{v_b}{v_s}[\exp(\beta\epsilon_{\alpha\beta}) - 1]\frac{1 - G_1\eta - G_2\eta^2}{(1-\eta)^3}, \tag{6}$$

where

$$G_1 = \frac{5}{2}\frac{3 + 8\frac{\delta}{\sigma} + 3\left(\frac{\delta}{\sigma}\right)^2}{15 + 4\frac{\delta}{\sigma}}, \tag{7}$$

$$G_2 = \frac{3}{2}\frac{12\frac{\delta}{\sigma} + 5\left(\frac{\delta}{\sigma}\right)^2}{15 + 4\frac{\delta}{\sigma}}. \tag{8}$$

The free energy per particle is, therefore,

$$\beta f = \beta f_{\mathrm{HS}} + \beta f_b, \tag{9}$$

which is a function of (η, T) only. In what follows we shall use the Carnahan–Starling approximation for f_{HS}.[35] Once in possession of the free energy, we can derive expressions for the pressure and the chemical potential and use them to find the phase diagram (binodal and spinodal lines) and critical point, as described in our previous papers.[25,26] The only difference is that we now also require the first three derivatives of $\Delta_{\alpha\beta}$ with respect to the packing fraction; these are easily evaluated and are listed in Appendix A, for completeness.

C. Percolation and cluster size distributions

1. Definitions

In a previous paper[27] we generalized the Flory theory of percolation to a model of associating (patchy) colloids consisting of hard spherical particles with f short-ranged attractive sites of m different types on their surfaces. Here, using the same theoretical framework,[27] we carry out a more detailed calculation for the case of $2A+1B$ sites (the simplest nontrivial case of dissimilar bonding sites), which corresponds to $m=2$, $f_A=2$, $f_B=1$, and $f \equiv f_A+f_B=3$.

We start by assuming that the finite clusters formed by the self-assembling particles are treelike (i.e., they have no loops) and define two sets of probabilities.

(i) $p_{\alpha\to\beta}$, the probability that a given site of type $\alpha(\alpha = A,B)$ is bonded to a site of type $\beta(\beta=A,B)$. These pair probabilities are related to the singlet probabilities p_A and p_B through the normalizations $p_\alpha = \Sigma_{\beta=A,B} p_{\alpha\to\beta}$ and can be written as functions of $n_{\alpha\beta}$, the number of bonds between sites of type α and sites of type β,

$$p_{\alpha\to\beta} = \frac{(1+\delta_{\alpha\beta})n_{\alpha\beta}}{f_\alpha N}. \tag{10}$$

(ii) Q_α, the probability that a given particle is not bonded to the infinite (percolated) cluster through one of its sites of type α; as a consequence, the probability to have a particle in a finite cluster is $P_s = \Pi_{\alpha=A,B} Q_\alpha^{f_\alpha}$.

Given these probabilities, we proceed to derive equations for the geometric or structural properties of the system: the percolation threshold, the probability that a given particle belongs to a finite cluster, the mean size, or number-averaged size, of the (finite) clusters, N_n, and the mean size of the (finite) cluster to which a randomly chosen particle belongs, or weight-averaged cluster size, N_w. We will then show how, through the laws of mass action, $p_{\alpha\to\beta}$ and Q_α can be obtained as functions of the density and temperature of the model fluid. We note that the patchy particle model considered here is known in literature of random networks as a "colored random graph"[36] and some of the results derived below may be derived using the methods of random graph theory.

2. Percolation threshold

We start by noting that the probability that a given particle is not connected to the infinite cluster is $Q_A^2 Q_B$ since it is not connected through any of its three independent bonding sites. The probabilities Q_α may be written in terms of p_α and $p_{\alpha\to\beta}$. As an example let us calculate Q_A. Consider a random particle and one of its A sites. The particle is not connected to the infinite cluster, through this site, if

(1) the A site is not bonded (with probability $1-p_A$);
(2) the A site is connected to another particle through an AB bond (with probability $p_{A\to B}$) and the other two A sites of the second particle are not connected to the infinite cluster (with probability Q_A^2);
(3) the A site is connected to another particle through an AA bond (with probability $p_{A\to A}$) and the remaining A and B sites of the second particle are not connected to the infinite cluster (with probability $Q_A Q_B$).

Then,

$$Q_A = (1-p_A) + p_{A\to B}Q_A^2 + p_{A\to A}Q_A Q_B. \tag{11}$$

Likewise, we find for Q_B,

$$Q_B = (1-p_B) + p_{B\to A}Q_A Q_B + p_{B\to B}Q_A^2. \tag{12}$$

These equations have the trivial solution $Q_A=Q_B=1$. When this is the only solution, there is no infinite cluster and the system is in the nonpercolated phase. When a second, nontrivial, solution exists, there is a nonzero probability of finding the particle in the infinite cluster, and the system is in the percolated phase. The percolation threshold may be found from a bifurcation analysis of the solutions of Eqs. (11) and (12). In what follows, however, we shall use a different method, which is also used to calculate N_w.

The finite treelike clusters can be constructed as a sequence of levels: Once a random particle is chosen as the "origin" of a (finite) cluster, each level is characterized by the number of bonded sites that connect it to the previous level (see Fig. 1). On a given level i there are $s_{A,i}$ and $s_{B,i}$ bonded sites of types A and B, respectively. The number of bonded A sites on level $i+1$ is calculated as follows. There are three distinct ways to connect level i of a finite cluster to a site A on the next level $i+1$.

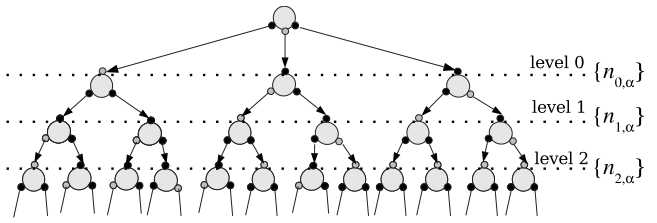

FIG. 1. Schematic representation of a tree cluster split into levels. The large circles are the particles, while the small circles (two black and one gray on each particle) represent the bonding sites (A and B, respectively). The lines between sites represent bonds that may occur with a prescribed probability $p_{\alpha\to\beta}$ (see the text). The arrows have no physical meaning: They just indicate the "direction" for counting cluster levels and particles.

(1) Starting at a B site on level i, through an $A\to A$ bond, given that the first A site of this bond is not connected to the infinite cluster, there are two A sites from where to start this bond.
(2) Starting at an A site on level i, through an $A\to A$ bond, given that the first A site of this bond is not connected to the infinite cluster.
(3) Starting at an A site on level i, through a $B\to A$ bond, given that the B site is not connected to the infinite cluster.

We then find

$$s_{A,i+1} = s_{A,i}(p^*_{B\to A} + p^*_{A\to A}) + 2s_{B,i}p^*_{A\to A}, \tag{13}$$

where $p^*_{\alpha\to\beta}$ is a conditional probability: the probability to find an $\alpha\to\beta$ bond given that site α is not connected to the infinite cluster. Since the fraction of α sites that is bonded to a β site and, through it, not bonded to an infinite cluster, is $p_{\alpha\to\beta}P_s/Q_\beta$, $p^*_{\alpha\to\beta}$ becomes

$$p^*_{\alpha\to\beta} = p_{\alpha\to\beta}\frac{P_s}{Q_\alpha Q_\beta}. \tag{14}$$

Notice that when the system is in a nonpercolated state (i.e., when $Q_\alpha = 1, \forall\,\alpha$), then $p^*_{\alpha\to\beta} = p_{\alpha\to\beta}$. Consequently, Eq. (13) may be rewritten as

$$s_{A,i+1} = s_{A,i}(Q_A p_{B\to A} + Q_B p_{A\to A}) + 2s_{B,i}Q_B p_{A\to A}. \tag{15}$$

Likewise, we find

$$s_{B,i+1} = s_{A,i}\left(Q_A p_{A\to B} + \frac{Q_A^2}{Q_B}p_{B\to B}\right) + 2s_{B,i}Q_A p_{A\to B}. \tag{16}$$

These two recursion relations are linear and may be written in matrix form,

$$\mathbf{s}_{i+1} = \mathbf{T}\mathbf{s}_i, \tag{17}$$

where $\mathbf{s}_i$ is a two-component column vector with entries $s_{A,i}$ and $s_{B,i}$, and $\mathbf{T}$ is a 2×2 matrix whose entries are the coefficients of Eqs. (15) and (16).

The matrix equation (17) is equivalent to two (identical) decoupled equations for the components of $\mathbf{s}_i$,

$$s_{\alpha,i+2} - Ts_{\alpha,i+1} + Ds_{\alpha,i} = 0, \tag{18}$$

where T and D are the trace and the determinant of $\mathbf{T}$, respectively, and $\alpha = A, B$. Equations (18) are "difference equations" that are easily solved to obtain $s_{\alpha,i}$, in terms of the eigenvalues of $\mathbf{T}(\lambda_\pm = T/2 \pm \sqrt{T^2-4D}/2)$. We distinguish the following two cases:

(i) Degenerate eigenvalues, $\lambda_+ = \lambda_- = \lambda$,

$$s_{\alpha,i} = (C_\alpha + B_\alpha i)\lambda^i. \tag{19}$$

(ii) Nondegenerate eigenvalues, $\lambda_+ \neq \lambda_-$,

$$s_{\alpha,i} = C_\alpha\lambda_+^i + B_\alpha\lambda_-^i. \tag{20}$$

In both cases, C_α and B_α are constants that depend on $s_{\alpha,0}$ and $s_{\alpha,1}$, and which are calculated using $s_{\alpha,0} = \Sigma_{\beta=A,B}f_\beta p_{\beta\to\alpha}P_s/(Q_\alpha Q_\beta)$ and $\mathbf{s}_1 = \mathbf{T}\mathbf{s}_0$. When $|\lambda_\pm| \leq 1$ both series (19) and (20) converge and the clusters are finite. It is easily shown that $\lambda_+ > 0$ and $\lambda_+ \geq |\lambda_-|$, and thus the percolation threshold occurs when

$$\lambda_+ = 1. \tag{21}$$

3. Cluster size distributions

The self-assembled finite clusters may be characterized by a size distribution $r(n)$, defined as the number of clusters of size n divided by the total number of particles in the system. For models with a single bonding probability (e.g., particles with f identical sites that bond with probability p), this distribution is known.[13,18,37] Some of its moments, however, may be calculated without knowledge of the form of $r(n)$.[19,38] The probability that a particle belongs to a finite cluster, $\Sigma_n nr(n)$, the mean cluster size,

$$N_n \equiv \frac{\Sigma nr(n)}{\Sigma r(n)}, \tag{22}$$

and the mean size of a cluster to which a randomly chosen particle belongs,[18]

$$N_w \equiv \frac{\Sigma n^2 r(n)}{\Sigma nr(n)}, \tag{23}$$

are three key physical quantities, related to the moments of $r(n)$, which may be calculated directly.

The probability that a particle belongs to a finite cluster is simply $Q_A^2 Q_B$ [and thus $\Sigma_n nr(n) = Q_A^2 Q_B$]. The calculation of N_n proceeds by recalling that under the no-loop assumption, the number of clusters is decreased by one when a bond is formed. Consequently, $N_n = 1/(1-n_b)$, where n_b is the mean number of bonds per particle in the finite clusters; because

$$n_b = \frac{1}{2}\sum_{\alpha=A,B} f_\alpha \sum_{\beta=A,B} p_{\alpha\to\beta}\frac{P_s}{Q_\alpha Q_\beta}, \tag{24}$$

then, using also Eqs. (11) and (12), we get

$$N_n = \frac{2}{2 - 2\left(\dfrac{Q_A - 1 + p_A}{Q_A}\right) - \left(\dfrac{Q_B - 1 + p_B}{Q_B}\right)}. \tag{25}$$

Calculation of N_w starts by choosing a particle randomly and considering the levels of the cluster to which the particle belongs (see Fig. 1). The number of particles on each level equals the number of bonded sites on that level, so

$$N_w = 1 + \sum_{i=0}^{\infty} (s_{A,i} + s_{B,i}). \tag{26}$$

To proceed, we need to distinguish the cases of degenerate and nondegenerate eigenvalues. It is straightforward to show that degenerate eigenvalues $\lambda_+ = \lambda_-$ occur when $p_{A\to A}=0$, corresponding to hyperbranched polymers or dimers, which we will not consider here. For the generic case of nondegenerate eigenvalues, we find, using Eq. (20), that the mean size of a cluster to which a randomly chosen particle belongs, Eq. (26), is

$$N_w = 1 + \frac{s_{A,0} + s_{B,0} - \frac{3}{2}D}{1 + D - T}, \tag{27}$$

where $s_{A,0}+s_{B,0}=\Sigma_{\alpha=A,B}\Sigma_{\beta=A,B} f_\beta p_{\beta\to\alpha} P_s/(Q_\alpha Q_\beta)$. As expected, N_w diverges at the percolation threshold as $\lambda_+ \to 1$. Note that both averages, Eqs. (25) and (27), have much simpler expressions in the nonpercolated regime (i.e., when $Q_A = Q_B = 1$).

The cluster size distribution, $r(n)$, may be calculated (at least formally) using the generating function formalism.[36,38] This is simply done in the limiting cases of random graphs (particles with identical bonding sites) or bipartite graphs (particles with distinct sites A and B and a single bonding probability), which correspond to the randomly branched and hyperbranched polymer models of Flory and Stockmayer, respectively. However, derivation of the cluster size distribution for random colored graphs (particles with distinct sites with two or more bonding probabilities) is far from trivial.

In what follows, we propose an ansatz for the distribution $r(n)$, which consists in mapping the model with distinct bonding sites of arbitrary functionality, onto an effective model, characterized by a—state dependent—functionality and a unique bonding probability. The mapping is defined through the requirement that N_n and N_w are the same for both models. These ratios of moments have been calculated above for our model; for models with arbitrary functionality and a single bonding probability, they are known (as well as the cluster size distribution function).

The cluster size distribution function of the effective model is given by[14,18]

$$r(n) = \bar{p}^{n-1}(1-\bar{p})^{(\bar{f}-2)n+2}\omega_n, \tag{28}$$

where

$$\omega_n = \frac{\bar{f}\Gamma((\bar{f}-1)n+1)}{\Gamma(n+1)\Gamma((\bar{f}-2)n+3)} \tag{29}$$

and Γ is the Gamma function. The size distribution, Eq. (28), is that of a model of particles with $\bar{f}$ identical sites and bonding probability $\bar{p}$;[13,14,18,37] $\bar{f}$ and $\bar{p}$ thus play the roles of *effective functionality* and *effective bonding probability*. Note that $\bar{f}$ need not be an integer[18] and, in general, it is not. The expressions for N_w and N_n within the effective model are (see Appendix B for a derivation)

$$N_n = \frac{2}{2 - \bar{f}\bar{p}\bar{Q}^{\bar{f}-2}} \tag{30}$$

and

$$N_w = 1 + \frac{\bar{f}\bar{p}\bar{Q}^{\bar{f}-2}}{1 - (\bar{f}-1)\bar{p}\bar{Q}^{\bar{f}-2}}, \tag{31}$$

where $\bar{Q}^{\bar{f}}$ is the probability that in the effective model, a particle belongs to a finite cluster; $\bar{Q}$ is related to $\bar{p}$ and $\bar{f}$ through (e.g., Ref. 18)

$$\bar{Q} = 1 - \bar{p} + \bar{p}\bar{Q}^{\bar{f}-1}. \tag{32}$$

$\bar{p}$ and $\bar{f}$ are now found by requiring that the sizes N_w and N_n from the effective model distribution equal those of the true model, i.e., by matching Eqs. (30) and (25), and Eqs. (31) and (27), and using Eq. (32); we obtain $\bar{p},\bar{f}$ [hence also Eq. (28)] as functions of the probabilities defined in Sec. II C 1. For the effective functionality we find

$$\frac{1}{\bar{f}} = 1 + \frac{1}{N_w - 1} - \frac{N_n}{2(N_n - 1)}, \tag{33}$$

which is thus independent of $\bar{p}$ and $\bar{Q}$. Notice that by matching of N_w, we ensure that the percolation threshold of the effective model will coincide with that of the true model. On the other hand, in the percolated phase, the normalization of the effective distribution $\bar{Q}^{\bar{f}}$ is not the same as that of the true distribution $Q_A^2 Q_B$.

4. Connection with thermodynamics

The geometrical percolation threshold, Eq. (21), N_n and N_w are exact, under the no-loop assumption, for a given set of probabilities $p_{\alpha\to\beta}$ (see Sec. II C 1). The model considered here is a fluid, and therefore the knowledge of the equilibrium bonding probabilities as functions of the density and temperature is required. An approximate relation between these probabilities and equilibrium thermodynamics results from regarding bond formation as an equilibrium chemical reaction.[27] For an $\alpha\beta$ bond between (independent) sites of types α and β, $\alpha+\beta \leftrightarrow \alpha\beta$ and chemical equilibrium imply

$$\frac{n_{\alpha\beta}}{(N_\alpha - n_\alpha)(N_\beta - n_\beta)} = \frac{\chi_{\alpha\beta}}{V}, \tag{34}$$

where $\chi_{\alpha\beta}$ is the equilibrium constant of the reaction, $\alpha\beta = AA, AB, BB$. N_α is the total number of bonding sites of type α, and n_α is the number of sites of type α that are bonded. Notice that $N_A = 2N_B = 2N$, $p_A = n_A/N_A$, and $p_B = n_B/N_B$. Substituting the probabilities $p_{\alpha\to\beta}$, given by Eq. (10), and p_α into Eq. (34), we find

$$p_{A\to A} = 2\eta\frac{2\chi_{AA}}{v_s}(1-p_A)^2, \tag{35}$$

$$p_{B\to B} = \eta\frac{2\chi_{BB}}{v_s}(1-p_B)^2, \tag{36}$$

$$p_{A\to B} = \eta \frac{\chi_{AB}}{v_s}(1-p_B)(1-p_A), \tag{37}$$

and $p_{B\to A}=2p_{A\to B}$. The equilibrium constants $\chi_{\alpha\beta}$ are now obtained by requiring consistency between the normalization of these probabilities (i.e., $p_A=p_{A\to A}+p_{A\to B}$ and $p_B=p_{B\to B}+p_{B\to A}$) and the laws of mass action of Wertheim's thermodynamic theory, Eqs. (2) and (3). A necessary and sufficient condition for this is[25]

$$\Delta_{\alpha\beta} = \frac{\chi_{\alpha\beta}}{v_s}(1+\delta_{\alpha\beta}), \tag{38}$$

where $\Delta_{\alpha\beta}$ are given by Eq. (4). We note that Wertheim's laws of mass action are nothing more than the normalization conditions of the probabilities $p_{\alpha\to\beta}$, with a specific approximation for the equilibrium constants.

In conclusion, once the density and temperature (and therefore $\Delta_{\alpha\beta}$) are fixed, the laws of mass action, Eqs. (2) and (3), provide the equilibrium probabilities p_α; the equilibrium probabilities $p_{\alpha\to\beta}$ then follow from Eqs. (35)–(38). The "geometric" or structural properties derived in this section can thus be calculated, at equilibrium, in terms of the fluid density and temperature.

III. MONTE CARLO SIMULATION

Data reported in this article are based on an extensive numerical study of the model introduced in Sec. II over a wide range of temperatures and densities. All results are for $\epsilon_{BB}=0$ and variable $\epsilon_{AB}/\epsilon_{AA}$. We employ several different methodologies. We perform standard Monte Carlo (MC) simulations in the *NVT* ensembles, using $N=6000$ particles, to elucidate the structure of the system and its connectivity. We perform grand canonical Monte Carlo (GCMC) simulations[39] to locate the liquid-vapor critical point. These calculations are complemented with histogram reweighting techniques to match the distribution of the order parameter $\rho-se$ with the known functional dependence expected for the Ising universality class critical point.[40] Here ρ is the number density, e is the potential energy density, and s is the mixing field parameter. We have not performed a finite-size study since we are only interested in the trends with varying ϵ_{AB}, but we have studied systems of different sizes, up to $L=15\sigma$. For each $\epsilon_{AB}/\epsilon_{AA}$ between 0.7 and 1.5, we calculated, using the methods described in Ref. 41, the critical temperature k_BT_c/ϵ_{AA} and critical density ρ_c.

We have also performed Gibbs-ensemble Monte Carlo (GEMC) simulations to map the coexistence curve. The GEMC method was designed[42] to study coexistence in the region where the liquid-vapor free energy barrier is sufficiently high to prevent crossing between the two phases. Using GEMC, we have studied a system of (total) 350 particles which partition themselves into the two boxes. At $T \ll T_c$, the vapor phase box contains only a few particles, while the remaining particles compose the liquid phase. We have also run tests with a total of $N=1000$ particles finding no differences. Equilibration at the lowest reported T required several months of computer time. The lowest T at which it is possible to reasonably equilibrate the system is set by the ratio $\max(|\epsilon_{AA}|,|\epsilon_{AB}|)/k_BT$. Indeed, the exponential of this ratio provides an indication of the number of attempts required to break an existing bond. With current numerical facilities, the boundary is around $\exp(20)\sim 5\times 10^8$. For this reason it was impossible to find coexistence for $\epsilon_{AB}<0.7$ or $\epsilon_{AB}>1.5$.

In all simulations, translational and rotational moves consisted of a random translation of $\pm 0.1\sigma$ and a random rotation of ± 0.1 rad of a randomly selected particle. Depending on the MC method, insertion and deletion moves (or swap moves) have been attempted, on average of every 500 displacement moves, and volume change moves (with volume changes of the order of $0.5\sigma^3$) every 100 motion moves.

To compute the cluster size distributions and connectivity properties, we define as bonded any pair of particles with a negative interaction energy, regardless of whether it is an *AA* or an *AB* bond. This choice is unambiguous due to the square-well (on-off) nature of the attractive interaction. Particles connected by an uninterrupted sequence of bonds are said to belong to the same cluster. Standard algorithms have been coded to partition all particles into different clusters. A cluster is said to be spanning if, taking into account periodic boundary conditions, it has an infinite mass. This is achieved by duplicating the system in each direction and checking that the cluster increases its mass. A state point is defined as percolating if more than 50% of its equilibrium configurations contain a spanning cluster.

IV. RESULTS

In this section we present results for fluids with $\epsilon_{BB}=0$ and a range of $\epsilon_{AB}/\epsilon_{AA}$ values, for which MC simulations were performed. Theoretical expressions for the phase diagrams and critical points have been calculated as described in our earlier papers,[25,26] except that we now use Eq. (5) for the radial distribution function rather than the simpler low-density approximation $g_{\mathrm{ref}}(\mathbf{r})=1$, in order to improve the quality of our predictions. We note that in the case under study ($\epsilon_{BB}=0$) one has $p_{B\to B}=0$, and, consequently the normalization relations allow calculation of the $p_{\alpha\to\beta}$ as functions of p_α. In fact, since $p_B=p_{B\to A}$ and, by definition, $p_{B\to A}=2p_{A\to B}$, one has

$$p_{A\to A} = p_A - p_B/2 = 1/2 - X_A - X_B/2 \tag{39}$$

and

$$p_{B\to A} = p_B = 1 - X_B. \tag{40}$$

We start by comparing, in Fig. 2, the predicted temperature and density dependence of X_A and X_B with corresponding quantities evaluated via MC simulations. Overall agreement is excellent, except for $\epsilon_{AB}/\epsilon_{AA}=1.5$, where small differences between theory and simulation are observed at low T; these differences are possibly caused by the formation of closed loops of four *AB*-bonded particles, which are favored by the bonding geometry. It is important to stress the difference between the cases $\epsilon_{AB}/\epsilon_{AA}<0.5$ and $0.5<\epsilon_{AB}/\epsilon_{AA}<1$. In the former case, X_B is always close to one, and indeed the theory predicts that it approaches one when $T\to 0$. Hence in this limit very few *B* sites are bonded. In the latter case, theory predicts (and MC data confirm) that X_B will instead

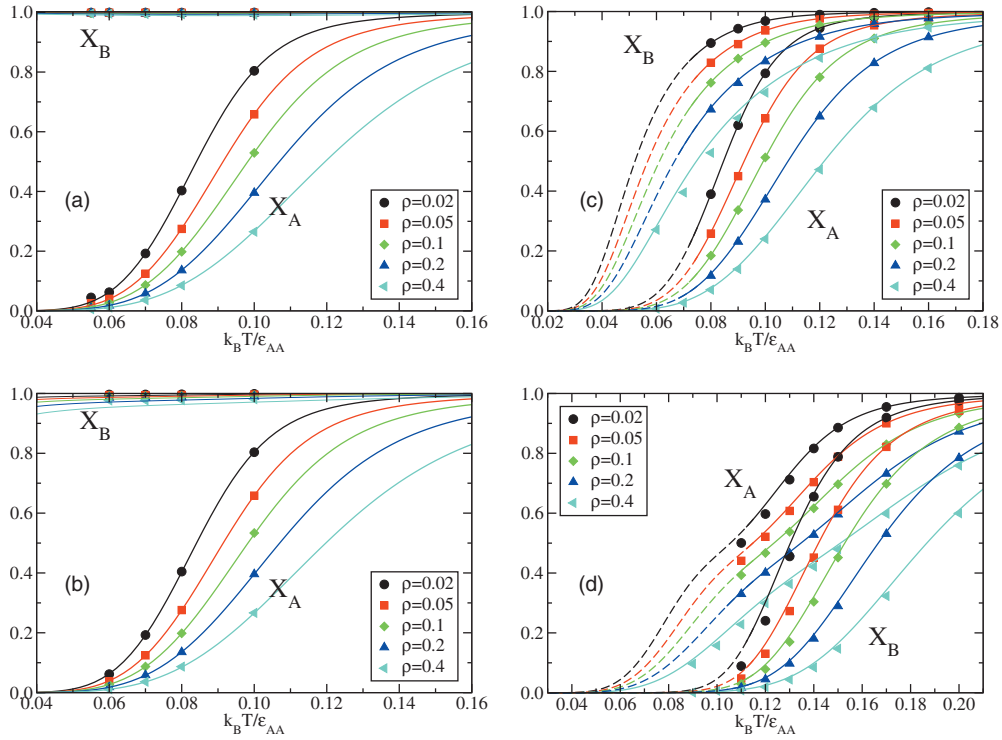

FIG. 2. Degrees of nonassociation of A and B. sites, X_A and X_B, vs temperature for $\epsilon_{BB}=0$ and (a) $\epsilon_{AB}/\epsilon_{AA}=0.45$; (b) $\epsilon_{AB}/\epsilon_{AA}=0.55$; (c) $\epsilon_{AB}/\epsilon_{AA}=0.8$; (d) $\epsilon_{AB}/\epsilon_{AA}=1.5$. Points are from simulation and lines are from theory; the latter are solid in the one-phase region and dashed in the two-phase region.

approach zero on deep cooling, and therefore that all B sites are bonded at low T. This difference can be rationalized by focusing on the lowest-energy state which can be achieved by the system. For $\epsilon_{AB}/\epsilon_{AA}<0.5$, this is an infinite chain of AA bonds, with no branching, whereas if $0.5<\epsilon_{AB}/\epsilon_{AA}<1$ the formation of all possible AB bonds is favored. This can be understood by noting that the system loses an energy ϵ_{AA} when an AA bond breaks, but gains $2\epsilon_{AB}$ if both free A ends join with two distinct B sites. Hence, the lowest-energy state of an N-particle system is $N\epsilon_{AB}+(N/2)\epsilon_{AA}$, which is indeed lower than the chain energy, $N\epsilon_{AA}$, when $0.5<\epsilon_{AB}/\epsilon_{AA}<1$.[26]

Next we focus on the ϵ_{AB}-dependence of the liquid-vapor critical parameters. Indeed, according to the theory,[26] by varying $\epsilon_{AB}/\epsilon_{AA}$ the system evolves from an ensemble of polydisperse AA-chains (when $\epsilon_{AB}/\epsilon_{AA}\ll 1$) to a nonpercolating assembly of hyperbranched aggregates (when $\epsilon_{AB}/\epsilon_{AA}\gg 1$). As a result, the critical density and temperature are expected to depend nonmonotonically on ϵ_{AB}. Figure 3 compares the theoretical and numerical results (also reported in Table I). The theory underestimates the density of the coexisting liquid phase but predicts the critical temperatures very accurately. The same type of agreement (on T_c) and disagreement (on ρ_c) was reported in the previous investigation on the functionality dependence of the critical parameters,[22] supporting the view that such behavior is intrinsic to the Wertheim approach. Moreover, the theory yields the correct nonmonotonic dependence of both the critical density ρ_c and the critical activity z_c on ϵ_{AB}. The significant drop in the critical density on decreasing ϵ_{AB} is reminiscent of the analogous trend observed in the study of the role of the functionality.[22] The analogy is not casual since decreasing ϵ_{AB} does make AB bonds less favorable, and thus acts as a reduction in the effective functionality. Only at very low T and for $\epsilon_{AB}/\epsilon_{AA}>0.5$, when almost all AA bonds have already formed, does X_B also approach zero [as shown in Fig. 2(c)] and the effective functionality of the particles go back to three. This reduction is also apparent in Fig. 3(b), where we plot the effective functionality, given by Eq. (33), calculated at the critical point. When $\epsilon_{AB}/\epsilon_{AA}\approx 1$, $\bar{f}_c\approx 3$, whereas when $\epsilon_{AB}/\epsilon_{AA}\ll 1$, $\bar{f}_c\to 2$. Finally, the energy per particle at the critical point E_c/N [see Fig. 3(c)] is underestimated (in absolute value) by theory, which also appears to predict a weak maximum.

Next we look in detail at the case $\epsilon_{AB}/\epsilon_{AA}=0.8$, starting with the potential energy in the system as a function of T and ρ. The energy per particle E/N can be written, in terms of X_A and X_B, as

$$\frac{E}{N}=\epsilon_{AA}\left(\frac{1}{2}-X_A+\frac{X_B}{2}\right)+\epsilon_{AB}(1-X_B), \tag{41}$$

where we have used Eqs. (35)–(37). The sigmoidal inflection in the T dependence of X_A and X_B previously discussed thus carries through to the T dependence of the energy, as shown in Fig. 4(a). This sigmoidal shape implies the presence of a maximum in the constant volume specific heat C_V,

$$C_v=\left(\frac{\partial E}{\partial T}\right)_V=-\epsilon_{AA}\left(\frac{\partial X_A}{\partial T}\right)_V+\left(\frac{1}{2}\epsilon_{AA}-\epsilon_{AB}\right)\left(\frac{\partial X_B}{\partial T}\right)_V. \tag{42}$$

As can be seen in Fig. 4(a), the theory predicts the internal energy very accurately. Figure 4(b) shows the specific heat calculated by differentiating numerically the theoretical curves (lines), and from fluctuations in the potential energy

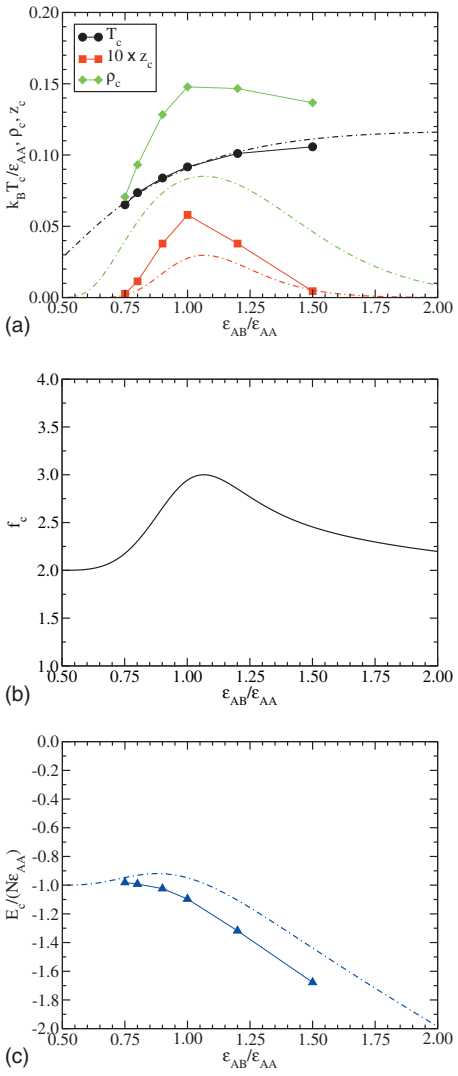

FIG. 3. Critical parameters for $\epsilon_{BB}=0$ and $\epsilon_{AB}/\epsilon_{AA}=0.8$. Symbols are from simulation and lines are from theory. (a) (Reduced) Critical temperature $k_B T_c/\epsilon_{AA}$, critical density ρ_c, and critical activity $z_c=\exp(\beta\mu_c)$; (b) effective functionality $\bar{f}_c$; (c) (reduced) critical energy per particle $E/(N\epsilon_{AA})$.

during the course of the MC runs (symbols). Again agreement is remarkably good.

The full phase diagram for $\epsilon_{AB}/\epsilon_{AA}=0.8$ is shown in Fig. 5. Besides the liquid-vapor critical point and the coexisting densities, we also plot the percolation line and the line of maxima of the specific heat at constant volume, C_V. The percolation line was determined as described in Sec. II. Also marked are the state points where, according to the MC simulation, the system percolates, in full agreement with the theoretical estimates for the percolation line. We further note, for future reference, that the critical point is located inside the percolation region, and that the line of C_V maxima, for $\epsilon_{AB}=0.8$, is located above the percolation curve.

TABLE I. Estimated critical parameters based on GCMC simulations complemented with histogram reweighting for the studied $\epsilon_{AB}/\epsilon_{AA}$ values. The last column gives the edge length of the simulation box.

$\epsilon_{AB}/\epsilon_{AA}$	T_c	ρ_c	z_c	L
0.75	0.064	0.064	0.000 22	13
0.80	0.074	0.093	0.001 14	14
0.90	0.084	0.134	0.003 79	13
1.00	0.092	0.147	0.005 81	12
1.20	0.101	0.146	0.003 81	12
1.50	0.106	0.137	0.000 45	11

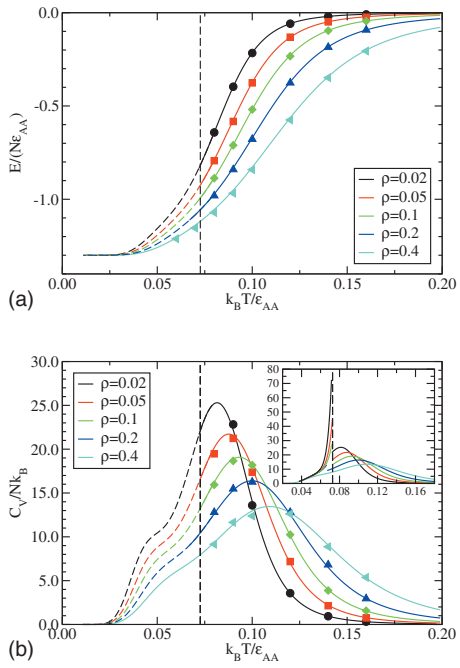

FIG. 4. (a) Internal energy and (b) specific heat at constant volume for $\epsilon_{AB}/\epsilon_{AA}=0.8$. The critical temperature is $k_B T_c/\epsilon_{AA}=0.0726$ (shown as the vertical dashed lines). Lines are from theory and symbols are from simulation; the latter are solid in the one-phase region and dashed in the two-phase region. In the inset we plot the specific heat calculated from an appropriately weighted internal energy in the two-phase region; it shows the typical discontinuity associated with the phase transition.

Figure 6 shows the phase diagrams and percolation lines for all $\epsilon_{AB}/\epsilon_{AA}$ values studied. Despite the fact that the theory underestimates the critical density and does not reproduce well the shape of the binodal curves close to the critical point, all relevant trends are recovered. Interestingly enough, according to both theory and numerical experiments, the density of the liquid phase converges toward a constant value $\rho\approx 0.4$ when $T\ll T_c$. This value is expected to be controlled by the density of a fully bonded equilibrium network of three-functional particles, in which all possible bonds are formed and the ground state of the system has been reached.

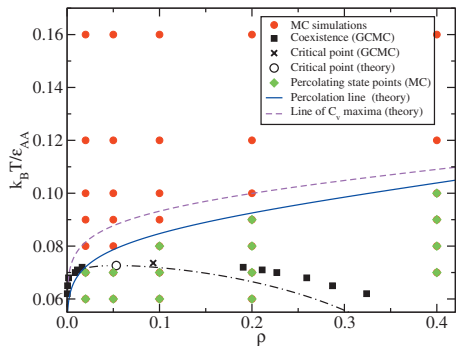

FIG. 5. Phase diagram for $\epsilon_{BB}=0$ and $\epsilon_{AB}/\epsilon_{AA}=0.8$ showing also the percolation line and the line of C_V maxima. Symbols are from simulation and lines are from theory.

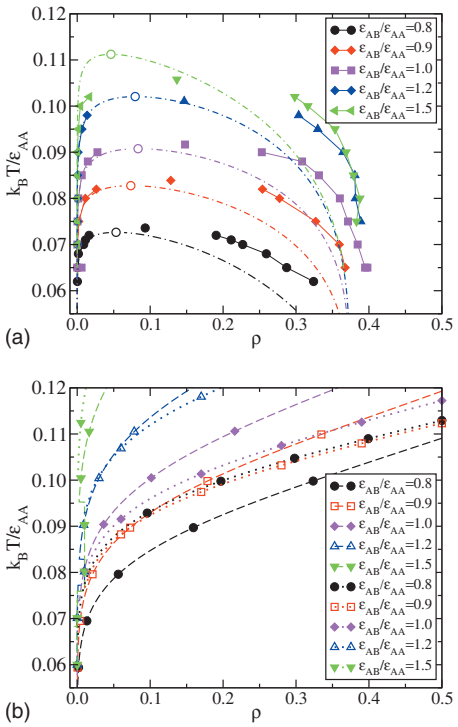

FIG. 6. (a) Phase diagrams for $\epsilon_{BB}=0$ and (from bottom to top) $\epsilon_{AB}/\epsilon_{AA}=0.8$, 0.9, 1.0, 1.2, and 1.5. Filled symbols connected by thin solid lines are from simulation and thicker dotted-dashed lines are from theory. We have also included the critical points from simulation (unconnected filled symbols) and from theory (open circles) to help with visualizing the critical behavior. (b) Percolation lines (dashed) and lines of C_v maxima (dotted) from theory, for the same systems as in (a).

Furthermore, as remarked in Refs. 24–26 and 43, the percolation line always intersects the vapor branch of the coexistence curve, i.e., at a density lower than the liquid-vapor critical density. This observation, which stresses that a percolating path of interactions is an essential ingredient for the development of critical fluctuations,[44] implies that the criticality of these systems involves two networked phases becoming identical, as previously suggested by Coniglio and co-workers.[21]

The maxima of C_V occur where the energy changes fastest with temperature at constant density; physically, they should signal the formation of a large number of interparticle bonds. Interestingly, the line of C_V maxima can be located either in the unpercolated region of the phase diagram (for $\epsilon_{AB}/\epsilon_{AA}=0.8$ and 1.5) or in the percolated region (for $\epsilon_{AB}/\epsilon_{AA}=0.9$, 1.0, and 1.2), whereas naively one would expect the onset of aggregation to always precede (i.e., occur at higher temperature for a fixed density) percolation. One possible explanation might be that for larger (smaller) $\epsilon_{AB}/\epsilon_{AA}$, the bonds that are formed in largest numbers are $AB(AA)$ bonds, which give rise to nonpercolating structures. These observations are consistent with results for the phase diagram of particles with varying number of *identical* sites:[24,43] It was found that on decreasing functionality, the C_V maxima move into the nonpercolating region. Indeed, in the case of equilibrium polymerization (functionality two), a line of C_V maxima is also present in the phase diagram[33] even though percolation is not possible owing to the absence of branching. Thus, in a first approximation, one can associate the

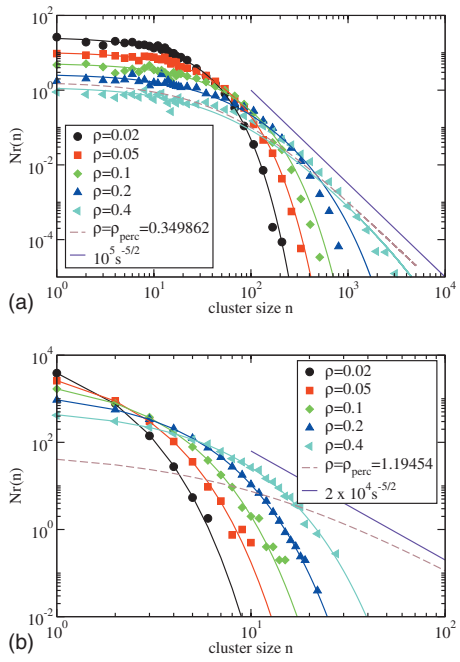

FIG. 7. Cluster size distributions for $\epsilon_{AA}=1$, $\epsilon_{BB}=0$, and $\epsilon_{AB}=0.45$, both above and below the percolation transition. The symbols are from simulation, the lines are calculated using our theory; $N=6000$ is the number of particles in the simulation box. (a) $k_BT/\epsilon_{AA}=0.06$; (b) $k_BT/\epsilon_{AA}=0.10$.

modulation of $\epsilon_{AB}/\epsilon_{AA}$ to a modulation of the effective functionality, consistently with the arguments presented when discussing the evolution of the critical parameters.

Figures 7 and 8 compare the cluster size distribution functions from simulation with the theoretical ansatz, Eq. (28), in both the nonpercolated and percolated states, going from the Y-junction ($\epsilon_{BB}=0$, $\epsilon_{AB}/\epsilon_{AA}\ll 1$) to the hyperbranched ($\epsilon_{BB}=0$, $\epsilon_{AB}/\epsilon_{AA}\gg 1$) limit.

In the nonpercolated state agreement is remarkable. No-

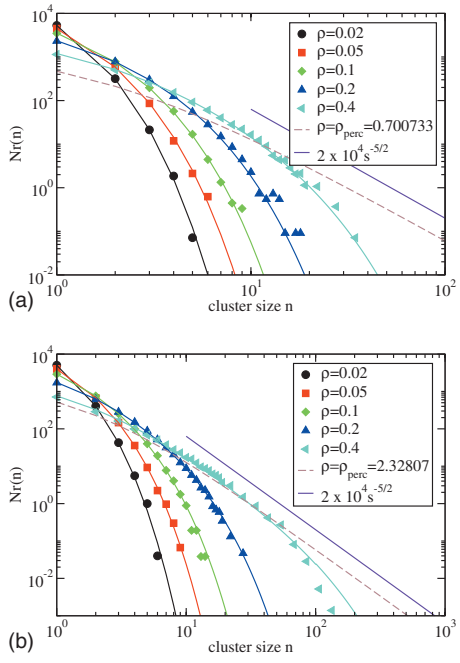

FIG. 8. Same as Fig. 7, but for $\epsilon_{AA}=1$, $\epsilon_{BB}=0$, and (a) $\epsilon_{AB}=0.8$, $k_BT/\epsilon_{AA}=0.12$; (b) $\epsilon_{AB}=1.5$, $k_BT/\epsilon_{AA}=0.17$.

tice, however, that the quality of this agreement is better for small clusters (for which the no-loop hypothesis is more accurate and the simulation results have less scatter). Moreover, very close to percolation [e.g., in Fig. 7(a), for $\rho=0.2,0.4$], the deviations between theory and simulation are due to the slight misprediction of the location of the percolation line, as well as to our neglect of critical fluctuations.

As mentioned earlier in Sec. II C 3, in the percolated states the effective distribution, Eq. (28), does not have the same normalization as the true model. This inconsistency was circumvented in the comparison between theory and simulations, by letting the number of clusters of size n be $NQ_A^2Q_B/\bar{Q}^f r(n)$ (where N is the number of particles in the simulation box).

V. CONCLUSIONS

The present article reports an extensive comparison between theoretical and numerical results for a very simple but quite rich model of interacting patchy particles with distinct interacting sites. The modeled particles have three attractive sites, two of type A and one of type B, interacting with energies $\epsilon_{AA}, \epsilon_{BB}$ and ϵ_{AB}. The richness of the model arises from the possibility of generating very different structures according to the relative values of ϵ_{ij}. We have focused on the case $\epsilon_{BB}=0$, for which, on varying the ratio $\epsilon_{AB}/\epsilon_{AA}$, the system evolves from an ensemble of linear polymers (whose exponential cluster size distribution is controlled by ρ and T) to an ensemble of nonpercolating hyperbranched polymers. In both these limits, a vapor-liquid transition is absent, in line with the impossibility of forming a percolating cluster. Consistently, the theory predicts that both on increasing and decreasing $\epsilon_{AB}/\epsilon_{AA}$ the critical density should approach zero. For $\epsilon_{AB}/\epsilon_{AA}=0.7$, the smallest value of the $\epsilon_{AB}/\epsilon_{AA}$ ratio for which we have been able accurately to estimate the critical parameters, $\rho_c=0.063$. This depression of the critical density is quite remarkable if compared to $\rho_c \approx 0.15$ for $\epsilon_{AB}/\epsilon_{AA} \approx 1$, or with $\rho_c \approx 0.47$, which is found for a (spherically symmetric) square-well potential with the same interaction range.[45] It should, however, be noted that all critical temperatures $k_B T_c/\epsilon_{AA} < 0.2$, and might therefore lie below the triple point temperature. To our knowledge, no studies of the phase diagram of the present model including crystal phases have been performed; hence it is impossible to know if here, the liquid state exists as a stable thermodynamic state or is only metastable. For the case of tetrahedral patchy particles, it was found that the vapor-liquid critical point becomes metastable with respect to the diamond crystal structure when the interaction range becomes about 20% of the particle diameter.[46,47] Similarly, it has been shown that a reduction in the patch width also favors the metastability of the crystal phase.[48]

According to theory, the case $\epsilon_{AB}/\epsilon_{AA}=0.5$ plays an important role. This value sets a crossover in the lowest-energy state that the system can achieve. Indeed, the ground state energy is $N\epsilon_{AA}$ for $\epsilon_{AB}/\epsilon_{AA}<0.5$ (an infinite chain of AA bonds, or equivalently $X_A=0$ and $X_B=1$) and $N\epsilon_{AB}+(N/2)\epsilon_{AA}$, when $0.5<\epsilon_{AB}/\epsilon_{AA}<1$.[26] In the latter range, all possible bonds in the system are formed (both X_A and X_B equal zero). As shown in Fig. 2, the ground state energy is almost reached at low T for all densities studied. Thus, as predicted theoretically and observed numerically, in this region the low T limit of the liquid branch of the vapor-liquid coexistence curve is found to be independent of the specific value of ϵ_{AB}, reflecting the lowest density which allows the formation of a fully bonded state.

The investigated model provides not only a test bed for the Wertheim theory but also allows one to identify the essential ingredients required for generating a liquid phase: Clearly an attraction between particles is a necessary, but not sufficient, condition for generating a critical point. The possibility of generating a percolating structure in the self-assembly process is indeed a prerequisite for vapor-liquid condensation.[49]

The present model is characterized by a clustering process which involves two types of bonds, generating a complex percolation problem. We have addressed this issue under the hypothesis that there are no closed loops of bonds in finite clusters. Interestingly, in this model in three dimensions, the number of closed loops of bonds is negligible, which allows us to perform a detailed comparison between numerical and theoretical expectations for the connectivity properties. The absence of intracluster bonds is a consequence of the low valence and arises from the entropic cost associated with the reduction of explored configurational space on closing the loop.[43] Because the strength of the AB interaction can be varied, the percolation process must be modeled with bonds of two different types. While a formal solution is possible for several average connectivity quantities (e.g., the mean cluster size and the mass of the infinite cluster),[27] an exact expression for the cluster size distribution has not been yet derived. In this manuscript we have shown that by mapping the percolation problem onto an equivalent one with a (state-dependent) average functionality and unique bonding probability, perfect agreement is found, in the unpercolated state, between theoretical predictions and numerical results for all cases in which bond loops are missing. The mapping is built by imposing the correct values for N_n and N_w at all densities and temperatures.

Finally we draw attention to a possible analogy between the present model and the dipolar hard sphere (DHS) fluid. Recent studies[50] suggest that DHSs are characterized by a low T-low ρ critical point as found here. Moreover, the structure of the system, as revealed by simulations, can be described in terms of long dipolar chains with thermally activated defects, providing branching points (Y-junctions) between chains, as in the present model. Zilman and Safran[51] suggested that the progressively lower concentration of Y-junctions on cooling may engender a phase diagram that pinches off at low temperature, i.e., in which at low T the density of the liquid branch decreases and approaches zero when $T \to 0$. Interestingly, in the limit where $\epsilon_{AA} \neq 0$, $\epsilon_{BB}=0$, and $\epsilon_{AB} \to 0$ (Y-junction limit[26]), our bonding free energy, Eq. (1), reduces, for sufficiently low temperatures, to the free energy of Zilman and Safran [compare Eq. (34) of Ref. 25 and Eq. (23) of Ref. 51, taking into account that Zilman and Safran's energy parameters are related to ours[25] via $\epsilon_e=\epsilon_{AA}/2$ and $\epsilon_j=-\epsilon_{AB}+\epsilon_{AA}/2$]. In this respect, it will be

particularly interesting to study some case where the present model might behave as proposed by Zilman and Safran, especially because the evaluation of the free energy based on the Wertheim theory does not require any fitting parameter. Work in this direction is underway.

ACKNOWLEDGMENTS

Financial supports from the Foundation of the University of Lisbon and the Portuguese Foundation for Science and Technology (FCT) under Contracts Nos. POCI/FIS/55592/2004, POCTI/ISFL/2/618, and PTDC/FIS/098254/2008 are gratefully acknowledged. F.S. acknowledges support from ERC-226207-PATCHYCOLLOIDS and ITN-234810-COMPLOIDS.

APPENDIX A: DENSITY DERIVATIVES OF $\Delta_{\alpha\beta}$

In this appendix we collect the density derivatives of the bond strengths $\Delta_{\alpha\beta}$, which are used in calculations of the phase diagram and critical point,

$$\frac{\partial \Delta_{\alpha\beta}}{\partial \eta} = \frac{3\Delta_{\alpha\beta}}{(1-\eta)} - \frac{v_b}{v_s}[\exp(\beta\epsilon_{\alpha\beta}) - 1]\frac{G_1 + 2G_2\eta}{(1-\eta)^3}, \quad \text{(A1)}$$

$$\frac{\partial^2 \Delta_{\alpha\beta}}{\partial \eta^2} = \frac{3\Delta_{\alpha\beta}}{(1-\eta)^2} + \frac{3}{(1-\eta)}\frac{\partial \Delta_{\alpha\beta}}{\partial \eta} - \frac{v_b}{v_s}[\exp(\beta\epsilon_{\alpha\beta}) - 1] \times \frac{3G_1 + 2G_2(1+2\eta)}{(1-\eta)^4}, \quad \text{(A2)}$$

$$\frac{\partial^3 \Delta_{\alpha\beta}}{\partial \eta^3} = \frac{6\Delta_{\alpha\beta}}{(1-\eta)^3} + \frac{6}{(1-\eta)^2}\frac{\partial \Delta_{\alpha\beta}}{\partial \eta} + \frac{3}{(1-\eta)}\frac{\partial^2 \Delta_{\alpha\beta}}{\partial \eta^2} - \frac{v_b}{v_s}[\exp(\beta\epsilon_{\alpha\beta}) - 1]\frac{12[G_1 + G_2(1+\eta)]}{(1-\eta)^5}. \quad \text{(A3)}$$

APPENDIX B: N_n AND N_w IN THE PERCOLATED REGION FOR THE MODEL WITH f IDENTICAL SITES

In this appendix we derive Eqs. (30) and (31) since we have not been able to find them in literature, in terms of $\bar{f}$, for the percolated phase (in Ref. 18 there are expressions for the particular case $\bar{f}=3$). This derivation is based on the results of Ref. 14 for the nonpercolated phase and on the definition, Eq. (32), of $\bar{Q}$.[18]

Let us write the size distribution, Eq. (28), as follows:

$$r(n) = \frac{(1-p)^2}{p}s(n), \quad \text{(B1)}$$

where

$$s(n) = \omega_n x^n, \quad \text{(B2)}$$

with ω_n given by Eq. (29) and

$$x = \bar{p}(1-\bar{p})^{\bar{f}-2}. \quad \text{(B3)}$$

In Ref. 14 the moments of $s(n)$, $S_i = \Sigma_{n=1}^{\infty} n^i \omega_n x^n$, are found for $\bar{p} < (p_c \equiv 1/[\bar{f}-1])$, i.e., for nonpercolated systems. Calculation of the moments of $r(n)$ for $p > p_c$ is done by taking into account the properties of the function $x(\bar{p})$ [Eq. (B3)]: $x(0) = x(1) = 1$ and a single maximum at $\bar{p} = p_c$. Hence for $\bar{p} > p_c$ there exists a p^* such that $0 < p^* < p_c$, $x(\bar{p}) = x(p^*)$, and $S_i(\bar{p}) = S_i(p^*)$. The first moment of the distribution function $r(n)$, i.e., the probability that a particle belongs to a finite cluster, can then be calculated for $\bar{p} > p_c$ using the expression for $S_1(p^*)$ of Ref. 14 and Eq. (B3),

$$\sum_{n=1}^{\infty} nr(n) = \frac{(1-p)^2}{p}S_1(p^*) = \left(\frac{1-\bar{p}}{1-p^*}\right)^{\bar{f}}. \quad \text{(B4)}$$

Combining Eq. (32), which relates $\bar{Q}$, $\bar{f}$, and $\bar{p}$, with the identity $\Sigma_{n=1}^{\infty} nr(n) \equiv \bar{Q}^{\bar{f}}$, a relation between $\bar{p}$ and p^* is obtained,

$$p^* = \bar{p}\bar{Q}^{\bar{f}-2}. \quad \text{(B5)}$$

Using this expression and the moments $S_i(p^*)$ from Ref. 14, Eqs. (30) and (31) follow.

[1] A. van Blaaderen, Nature (London) **439**, 545 (2006).
[2] V. N. Manoharan, M. T. Elsesser, and D. J. Pine, Science **301**, 483 (2003).
[3] D. J. Kraft, J. Groenewold, and W. K. Kegel, Soft Matter **5**, 3823 (2009).
[4] A. B. Pawar and I. Kretzschmar, Macromol. Rapid Commun. **31**, 150 (2010).
[5] P. I. C. Teixeira, J. M. Tavares, and M. M. Telo da Gama, J. Phys.: Condens. Matter **12**, R411 (2000).
[6] W. G. Chapman, K. E. Gubbins, G. Jackson, and M. Radosz, Fluid Phase Equilib. **52**, 31 (1989).
[7] E. Zaccarelli, J. Phys.: Condens. Matter **19**, 323101 (2007).
[8] M. S. Wertheim, J. Stat. Phys. **35**, 19 (1984).
[9] M. S. Wertheim, J. Stat. Phys. **35**, 35 (1984).
[10] M. S. Wertheim, J. Stat. Phys. **42**, 459 (1986).
[11] M. S. Wertheim, J. Stat. Phys. **42**, 477 (1986).
[12] K. S. Schweizer and J. G. Curro, Adv. Polym. Sci. **116**, 319 (1994).
[13] P. J. Flory, *Principles of Polymer Chemistry* (Cornell University Press, Ithaca, 1981).
[14] W. H. Stockmayer, J. Chem. Phys. **11**, 45 (1943).
[15] M. Cohen and A. B. Harris, Phys. Rev. E **78**, 041116 (2008).
[16] T. L. Hill, *Statistical Mechanics* (McGraw-Hill, New York, 1956).
[17] M. E. Fisher and J. W. Essam, J. Math. Phys. **2**, 609 (1961).
[18] M. Rubinstein and R. H. Colby, *Polymer Physics* (Oxford University Press, Oxford, 2003).
[19] D. Stauffer and A. Aharony, *Introduction to Percolation Theory*, revised 2nd ed. (Taylor & Francis, London, 1994).
[20] J. L. Spouge, Macromolecules **16**, 121 (1983).
[21] A. Coniglio, U. De Angelis, A. Forlani, and G. Lauro, J. Phys. A **10**, 219 (1977).
[22] E. Bianchi, J. Largo, P. Tartaglia, E. Zaccarelli, and F. Sciortino, Phys. Rev. Lett. **97**, 168301 (2006).
[23] G. Foffi and F. Sciortino, J. Phys. Chem. B **111**, 9702 (2007).
[24] E. Bianchi, P. Tartaglia, E. Zaccarelli, and F. Sciortino, J. Chem. Phys. **128**, 144504 (2008).
[25] J. M. Tavares, P. I. C. Teixeira, and M. M. Telo da Gama, Mol. Phys. **107**, 453 (2009).
[26] J. M. Tavares, P. I. C. Teixeira, and M. M. Telo da Gama, Phys. Rev. E **80**, 021506 (2009).
[27] J. M. Tavares, P. I. C. Teixeira, and M. M. Telo da Gama, Phys. Rev. E **81**, 010501(R) (2010).
[28] K. Van Workum and J. F. Douglas, Phys. Rev. E **71**, 031502 (2005).
[29] G. Jackson, W. G. Chapman, and K. E. Gubbins, Mol. Phys. **65**, 1 (1988).
[30] D. Ghonasgi, V. Perez, and W. G. Chapman, J. Chem. Phys. **101**, 6880 (1994).
[31] R. P. Sear and G. Jackson, J. Chem. Phys. **105**, 1113 (1996).
[32] L. González MacDowell, M. Müller, C. Vega, and K. Binder, J. Chem. Phys. **113**, 419 (2000).
[33] F. Sciortino, E. Bianchi, J. F. Douglas, and P. Tartaglia, J. Chem. Phys. **126**, 194903 (2007).

[34] I. Nezbeda and G. Iglesia-Silva, Mol. Phys. **69**, 767 (1990).
[35] N. F. Carnahan and K. E. Starling, J. Chem. Phys. **51**, 635 (1969).
[36] B. Söderberg, Phys. Rev. E **68**, 015102 (2003).
[37] P. J. Flory, J. Am. Chem. Soc. **63**, 3083 (1941).
[38] M. E. Newman, S. H. Strogatz, and D. J. Watts, Phys. Rev. E **64**, 026118 (2001).
[39] B. Smith and D. Frenkel, *Understanding Molecular Simulations* (Academic, New York, 1996).
[40] N. B. Wilding, J. Phys.: Condens. Matter **9**, 585 (1997).
[41] F. Romano, P. Tartaglia, and F. Sciortino, J. Phys.: Condens. Matter **19**, 322101 (2007).
[42] A. Z. Panagiotopoulos, Mol. Phys. **61**, 813 (1987).
[43] E. Bianchi, P. Tartaglia, E. La Nave, and F. Sciortino, J. Phys. Chem. B **111**, 11765 (2007).
[44] A. Coniglio and W. Klein, J. Phys. A **13**, 2775 (1980).
[45] J. Largo, M. A. Miller, and F. Sciortino, J. Chem. Phys. **128**, 134513 (2008).
[46] F. Romano, E. Sanz, and F. Sciortino, J. Phys. Chem. B **113**, 15133 (2009).
[47] F. Romano, E. Sanz, and F. Sciortino, J. Chem. Phys. **132**, 184501 (2010).
[48] A. Giacometti, F. Lado, J. Largo, G. Pastore, and F. Sciortino, J. Chem. Phys. **132**, 174110 (2010).
[49] F. Sciortino, A. Giacometti, and G. Pastore, Phys. Rev. Lett. **103**, 237801 (2009).
[50] G. Ganzenmüller and P. J. Camp, J. Chem. Phys. **126**, 191104 (2007).
[51] A. G. Zilman and S. A. Safran, Phys. Rev. E **66**, 051107 (2002).